Experimental FWA MIMO Capacity Analysis in 6 and 37 GHz Bands

A technical paper prepared for presentation at SCTE TechExpo24

Roy Sun
Ph.D., Principal Architect
CableLabs
r.sun@cablelabs.com

Dorin Viorel
Distinguished Technologist
CableLabs
d.viorel@cablelabs.com

Wilhelm Keusgen
Ph.D., Professor
Technische Universität Berlin
wilhelm.keusgen@tu-berlin.de

Table of Contents

List of Figures

List of Tables

1. Introduction

5G Fixed Wireless Access (FWA) has been deployed by operators for several years. In the North American markets, Mobile Network Operators (MNOs) increased their market share at the expense of cable-based services of Multiple Systems Operators (MSOs). Conversely, MSOs also enter the FWA space, utilizing licensed, unlicensed, shared bands.

As the data demand keeps increasing, the spectrum resources become congested and more costly. The 6 GHz band from 5.925 to 7.125 GHz was released by the U.S. Federal Communications Commission (FCC) for unlicensed use in 2020 [1]. The lower-37 GHz band from 37 to 37.6 GHz and lower-42 GHz band from 42 to 42.5 GHz are being considered for sharing [2]. FWA networks typically use outdoor small cells and indoor cells to offload macro cells, and these FWA cells are more feasible to share the spectra. FWA use cases monetize under-utilized spectra becoming available as the result of the large channel bandwidth mid-band spectra.

CableLabs began evaluating the FWA case multiple years ago, and references [3]-[7] are some of their recent publications. While developing FWA simulation studies, the CableLabs team identified the potential impact of the radio propagation channel on FWA coverage and ultimately quality of service. Five measurement campaigns were designed to characterize channels in FWA scenarios in the 6 and 37 GHz bands:

1. The first measurement campaign was conducted in an indoor office environment [8] in June 2022, in which the root-mean-square (RMS) delay spread (RMS-DS), RMS angular spread (RMS-AS), Rician *K*-factor, channel characteristics over different synthetic beamwidth, and spatial correlation were reported.
2. The second campaign (Sept. 2022) moved to an outdoor-to-indoor (O2I) environment [9] and [10]. The O2I loss, tree loss, small-scale fading Rician *K*-factor, angle of arrival (AoA), and optimized customer premises equipment (CPE) location outside or inside a residential house were analyzed.
3. The third measurement campaign (May 2023) was extended from the first campaign to 76 transmitter (TX) locations throughout the 2nd floor of the CableLabs office building [11], extracting an indoor path loss model compared with 3GPP models.
4. The fourth campaign (June 2023) extended the indoor study from 1×1000 single-input multiple-output (SIMO) to 2×1000 multiple-input multiple-output (MIMO) antenna systems to evaluate the MIMO capacity in an indoor propagation channel [12].
5. The fifth campaign (Sept. 2023) studied the MIMO capacity in an O2I environment [13].

The first three campaigns [8]-[11] for SIMO channel measurements are summarized in a companion paper [14]. This paper summarizes the MIMO channel measurements [12] and [13].

2. Key Findings

MIMO not only forms a high gain to compensate for the path loss, but multi-user MIMO (MU-MIMO) could also increase the capacity in a diverse propagation channel. The key findings include:

1. MIMO capacity gain:
    - The theoretical 2×2 MIMO capacity gain is 2.

- The measured 2×2 MIMO capacity gain is 1.7 in line-of-sight (LOS) conditions in an O2I environment, and 1.8–1.9 in non-LOS (NLOS) conditions in an O2I environment, and it is 1.9 in an indoor environment regardless of LOS or NLOS conditions.

2. MIMO capacity gain versus antenna separation distance:

    - MIMO capacity gain is not strongly dependent on antenna separation distance, which is true on both the TX and receiver (RX) sides.

3. MIMO capacity gain versus CPE orientation:

    - Orientation does not matter due to rich scattering, and variation of MIMO capacity gain is not dependent on CPE orientation.

4. Correlations between MIMO capacity gain and other channel characteristics:

    - The MIMO capacity gain is positively correlated with the number of MPCs, RMS-AS, and RMS-DS.

    - The MIMO capacity gain is negatively correlated with the variation of MIMO capacity gain, channel covariance, and Rician *K*-factor.

3. Measurement Campaign

3.1. MIMO Channel Sounding System

The MIMO channel sounding system consists of two transmitters, one receiver on a virtual circular array (VCA), and a synchronization system. The two TXs are synchronized and transmit two orthogonal Frank-Zadoff-Chu sequences. The autocorrelation gain of the signals is 54 dB based on a sequence length of 250 thousand samples. The mutual interference of the orthogonal sequences reduces the processing gain to 51 dB. Vertical polarized open waveguides are used on TXs, the maximum gain is 7.2 dBi for 6 GHz and 8 dBi for 37 GHz, the horizontal half-power beamwidth is approximately 70° for 6 GHz and 54° for 37 GHz, the vertical half-power beamwidth is approximately 122° for 6 GHz and 120° for 37 GHz.

An omnidirectional antenna sits on a VCA on the receiver side and it collects 1000 channel impulse responses (CIRs) while the VCA moves on a complete circumference within half a second. The diameter of the VCA is 15 cm for 6 GHz and 5 cm for 37 GHz. In the post-processing, two RX positions, which have a pre-defined separation distance (e.g., of two wavelengths) on the VCA, are paired to mimic a 2-element MIMO RX antenna. In this way, 1000 different antenna pairs, each having same separation but different orientation, can be defined and for each one a channel matrix is estimated. The channel matrices are the bases of further statistical analyses of channel capacity and MIMO gain. Additionally, the information from all 1000 RX antennas together can be used to estimate the main directions of arrival and to find significant multipath components, giving further insights in the properties of the MIMO radio channel. The conducted power at TXs' antenna port is 26 dBm for both frequencies. The bandwidth is 500 MHz corresponding to a 2 ns delay resolution. The center frequencies are 6.175 GHz in the 6 GHz which exactly overlaps the U-NII-5 band from 5.925 to 6.425 GHz, and 37.3 GHz in the 37 GHz which overlaps the majority segment of the 37–37.6 GHz shared band. More detailed information on the SIMO sounder is provided in [8]-[11], and the information for the MIMO sounder is presented in [12] and [13].

3.2. Indoor-Office Environment

Measurement campaign #4 was conducted on the 2nd floor of the CableLabs office building in Louisville, Colorado USA. The floor plan and test positions (TPs) are shown in Figure 1, and photos of the fixed TX position (red circle) in and Figure 1one of the RX positions (green circles) are presented in Figure 2. The TX antennas are mounted 2.6 m above ground mimicking a ceiling-mount indoor base station (BS) or Wi-Fi access point (AP). The RX and VCA are on a cart with an antenna 1.2 m above ground, mimicking a cellphone or laptop user. The cart was relocated to 17 TPs to repeat data collection. Nothing was moving during the data collection. TP8 and TP9 were in the same position, TP8 with the door to the separated laboratory (Akron Lab) open in an LOS condition, and TP9 with the door closed. The interior walls (double-line in the floor plan) are drywall. The exterior wall of the building is made from bricks.

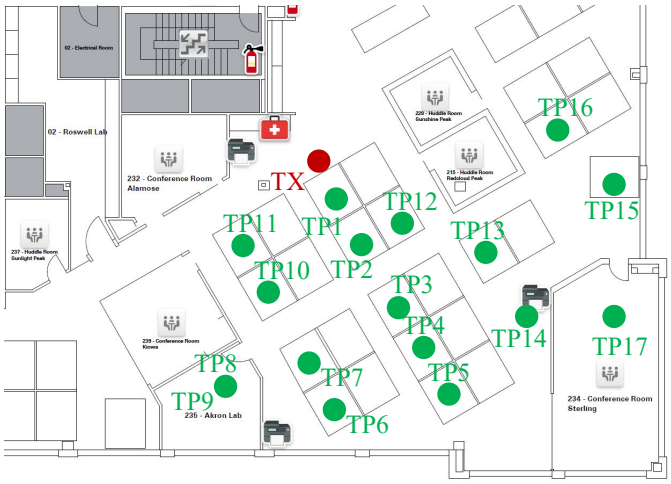

Figure 1 - Floor plan and test positions in an indoor environment [12]

(a) **(b)**

Figure 2 - Photos of (a) TXs; and (b) RX at test position 17

3.3. Outdoor-to-Indoor Environment

Measurement campaign #5 took place in a typical North American residential single-family house in Brighton, Colorado USA. The house is made of wood structure, drywalls, and wood exterior sidings. The aerial view of the house and the outdoor TX positions are illustrated in Figure 3. The TX antennas were

mounted 5 m above ground outdoors mimicking a pole-mount or strand-mount microcell BS. TX1 was 10 m from the house in LOS condition. TX positions 2–4 were located approximately 45 m away from the house. TX2 has LOS condition towards the house. TX3 was blocked by one aspen tree, TX4 was blocked by two spruce trees and one maple tree. The floor plan of the house and the 17 RX test positions are shown in Figure 4. RX position 0 was outdoors on the backyard patio (first floor) of the house, it has a clear LOS condition to TX1 and TX2. Eight RX positions, 1–8, were indoors on the first floor. Another eight RX positions, 9–16, were indoors on the second floor. All 16 indoor RX positions mimic potential CPE positions inside a house in an FWA deployment scenario and were separated by at least one wall from the TX positions, resulting in NLOS channel conditions. The RX including VCA were on a cart, similar to Figure 2(b), 1.2 m above ground.

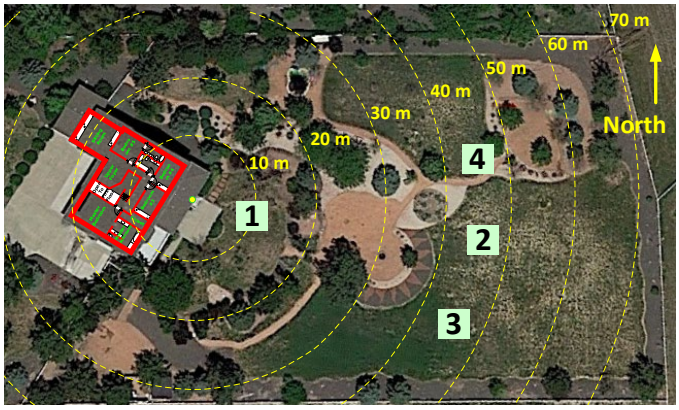

Figure 3 - Aerial view of the measurement site showing the four outdoor TX TPs [13]

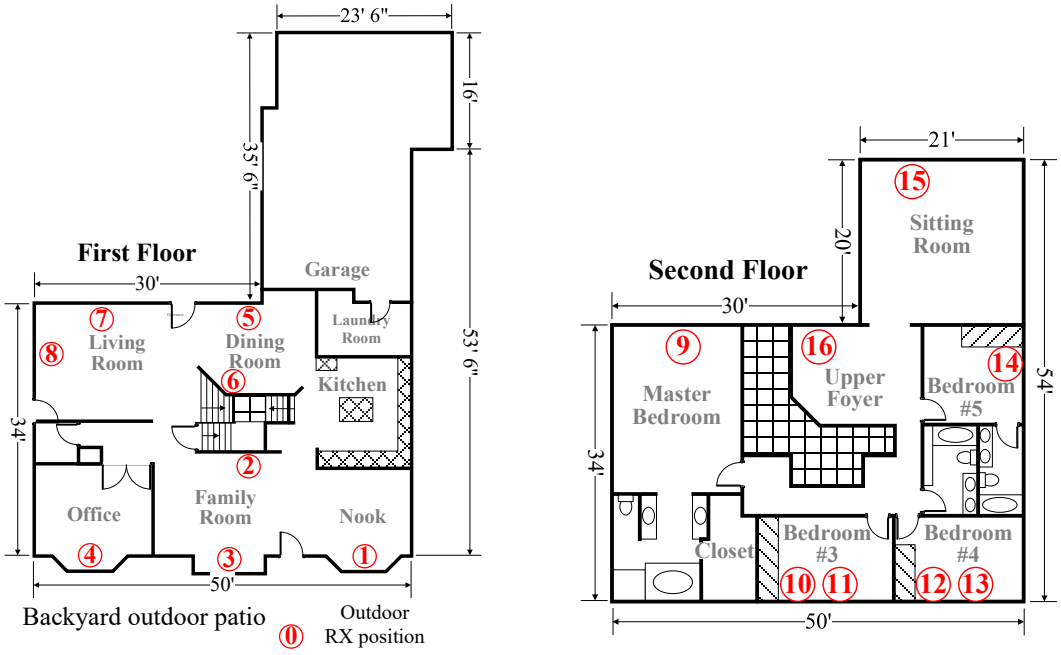

Figure 4 - Floor plan of the house, showing 16 indoor and one outdoor RX test positions (a) first floor; and (b) second floor [13]

4. MIMO Capacity Evaluation Methods

A single-input single-output (SISO) channel can be described as

$$y = xh + n, \tag{1}$$

where x is the transmit signal, y is the receive signal, h is the channel gain, and n denotes the noise. The theoretical SISO channel capacity, C, follows the classic Shannon limit:

$$C = B\log_2\left(1 + \frac{\sigma_x^2}{\sigma_n^2}h\right) = B\log_2(1 + \mathrm{SNR}), \tag{2}$$

where B is the channel bandwidth, σ_x^2 denotes the transmit power, σ_n^2 the noise power and SNR is the signal-to-noise ratio at the receiver.

A 2×2 MIMO channel is presented in Figure 5, which is described mathematically as:

$$\mathbf{y} = \mathbf{H}\boldsymbol{x} + \boldsymbol{n}, \tag{3}$$

where **x** and **y** are vectors representing signals at TXs and RXs, respectively, $\boldsymbol{n}$ is noise, and **H** is the channel matrix. **H** is normalized by the channel gain, G, per TP, resulting in $\widehat{\mathbf{H}} = \frac{\mathbf{1}}{\sqrt{G}}\mathbf{H}$. The MIMO channel capacity follows:

$$C = B\log_2\left(\det\left[\mathbf{I}_{N_R} + \frac{\mathrm{SNR}}{N_R}\widehat{\mathbf{H}}\widehat{\mathbf{H}}^H\right]\right), \tag{4}$$

where $\mathbf{I}_{N_R}$ is the identity matrix of dimension N_R, and $N_R = 2$ denotes the number of receive antennas. A detailed description of the method is provided in [13]. In our measurement campaigns, the channel matrix **H** is measured, based on which the MIMO capacity is derived. Furthermore, the SISO capacities are estimated for comparison, which is evaluated from each of the four entries of $\widehat{\mathbf{H}}$. and being averaged.

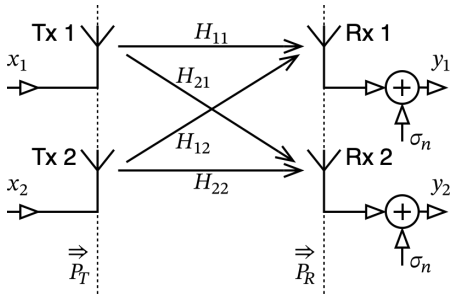

Figure 5 - A 2×2 MIMO channel [13]

5. MIMO Capacity Measurement Results

5.1. Example Results

The channel sounder collects CIRs. An example of its power version, the power delay profile (PDP)is illustrated in Figure 6(a) Here, the TP 0 (outdoor) and Rx position 1 (Rx1) are chosen, which define a LOS channel. By applying the fast Fourier transform (FFT), the corresponding channel transfer functions (CTFs) of the four channels between two TXs and two RXs are shown in Figure 6(b). Figure 7(a) and (b) present the SISO and MIMO capacity, respectively, for this TP along with the variation ranges from the 20th to 80th percentile, as well as from the 5th to 95th percentile. The channel capacity increases over SNR. The variation stems from the results for the 1000 different MIMO antenna configurations, as described above. Additionally, the MIMO capacity gain, as the ratio between MIMO and SISO capacity in percentage, is shown in Figure 8 The mean MIMO capacity gain ranges from 1.6 to 1.8 with a large variation across the antenna configurations..

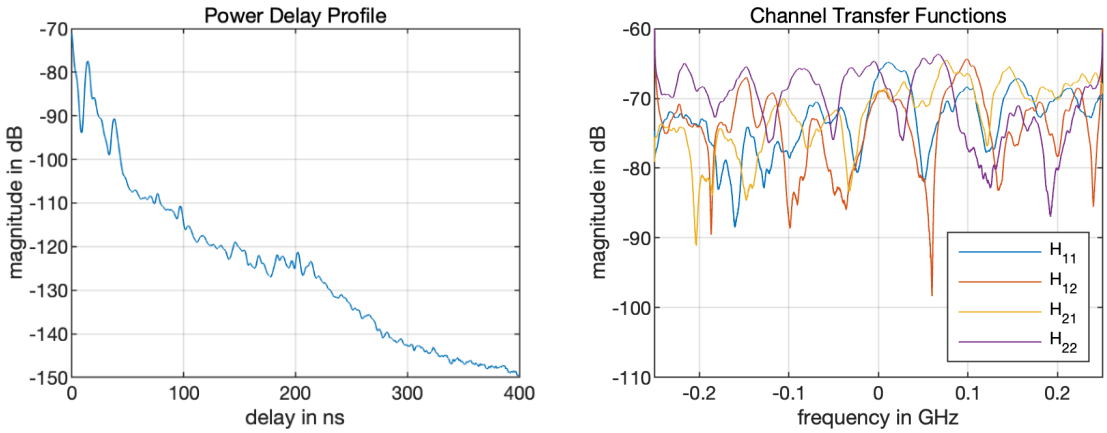

(a) (b)

Figure 6 - An example (a) PDP and (b) CTF for TX1, RX0 at 6 GHz [13]

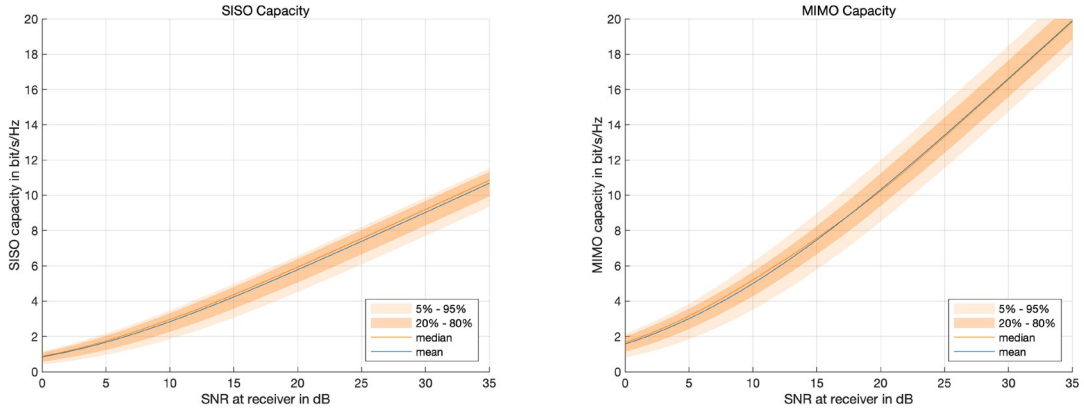

(a) (b)

Figure 7 - Normalized capacity and its 5% - 95% and 20% - 80% quantiles for (a) SISO; and (b) MIMO for TX1, RX0 at 6 GHz

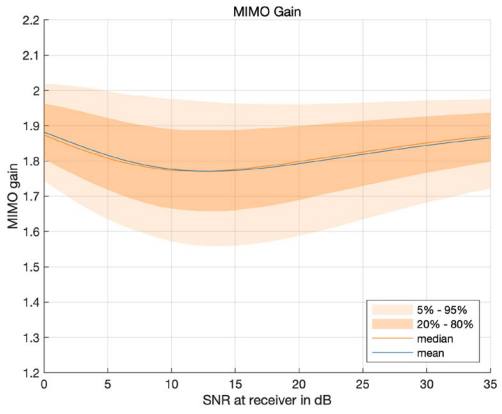

Figure 8 - MIMO / SISO capacity gains at 6 GHz for TX1, RX0 in the LOS scenario

5.2. MIMO Capacity Gain Statistics

The mean MIMO capacity gain for both O2I and indoor environments and both 6 GHz and 37 GHz frequencies are summarized in Table 1. **The theoretical 2×2 MIMO capacity gain is 2. The measured 2×2 MIMO capacity gain is 1.7 in O2I LOS conditions, 1.8–1.9 in O2I NLOS conditions, and for indoor again 1.8–1.9 in both LOS and NLOS conditions.** This is likely because the O2I LOS condition has a strong dominant direct path and the MPCs are relatively weak and sparse. The spatial diversity of the O2I LOS channel is low, and the MIMO capacity gain is relatively small. As moving from O2I LOS to NLOS condition, the dominant MPC becomes relatively weaker compared with other MPCs or there is no dominant MPC. Thus, the spatial diversity increases, and MIMO capacity gains achieve 1.84 at 37 GHz and 1.91 at 6 GHz which are close to the theoretical maximum value of 2. In the indoor environment, MPCs are rich due to reflections from walls, ceilings, ground, and furniture. Even in LOS conditions, rich scatterers provide sufficient diversity in the propagation channel that yields a MIMO capacity gain of nearly 1.9.

Table 1 - Mean MIMO capacity gain

		Mean MIMO capacity gain	
		LOS	NLOS
O2I	6 GHz	1.67	1.91
	37 GHz	1.68	1.84
Indoor	6 GHz	1.91	1.93
	37 GHz	1.86	1.90

The results in Table 1 are based on antenna separation distance of 2λ at TXs and 2λ at RX in O2I and 4λ at TXs and 4λ at RX in the indoor environment. To compare the impact of antenna separation, the indoor measurements were done with different TX antenna spacing of 2λ, 4λ, and 8λ at 6 GHz and 3λ, 4λ, 8λ at 37 GHz. Due to the dimensions of the open waveguides, the spacing cannot be smaller than 2λ at 6 GHz or smaller than 3λ at 37 GHz. Because 1000 RX antenna positions were measured on a VCA, the RX antenna separation distance is limited by the diameter of the VCA, which is 30 cm (approximately 6λ) at 6 GHz and 10 cm (approximately 12λ) at 37 GHz. The MIMO capacity gain results versus multiple TX and RX antenna separation distances are listed in Table 2. **The MIMO capacity gain is not strongly dependent on antenna separation distance.**

Table 2 - Indoor mean MIMO capacity gain versus antenna separation distance [12]

			MIMO capacity gain		
			Min	Mean	Max
6 GHz	LOS	2λ (TX), 2λ (RX)	1.73	1.87	1.94
		4λ (TX), 4λ (RX)	1.85	1.91	1.94
		8λ (TX), 6λ (RX)	1.86	1.92	1.94
	NLOS	2λ (TX), 2λ (RX)	1.92	1.93	1.94
		4λ (TX), 4λ (RX)	1.86	1.92	1.94
		8λ (TX), 6λ (RX)	1.93	1.94	1.94
37 GHz	LOS	3λ (TX), 3λ (RX)	1.80	1.86	1.94
		4λ (TX), 4λ (RX)	1.77	1.87	1.94
		8λ (TX), 8λ (RX)	1.82	1.89	1.94
	NLOS	3λ (TX), 3λ (RX)	1.74	1.86	1.94
		4λ (TX), 4λ (RX)	1.74	1.90	1.94
		8λ (TX), 8λ (RX)	1.73	1.90	1.94

5.3. MIMO Capacity Gain vs. CPE Orientation

A practical issue for operators is optimizing the CPE antenna array orientation to maximize coverage and throughput. A professional installer may be required to go to consumers' homes to find the best CPE orientation. This increases the overall installation costs and reduces the operator's margin. In this subsection, we will provide a quantitative analysis of this issue, especially regarding optimizing MIMO capacity gain. The MIMO capacity gain vs. 360 azimuth angles for an indoor LOS test position (TP 12, see Figure 1) with 12 dB SNR are shown in Figure 9. The MIMO capacity gain varies in a small range, and it varies fast over azimuth angle. **There is no need and no way for operators to optimize the CPE orientation in a rich scattering environment.**

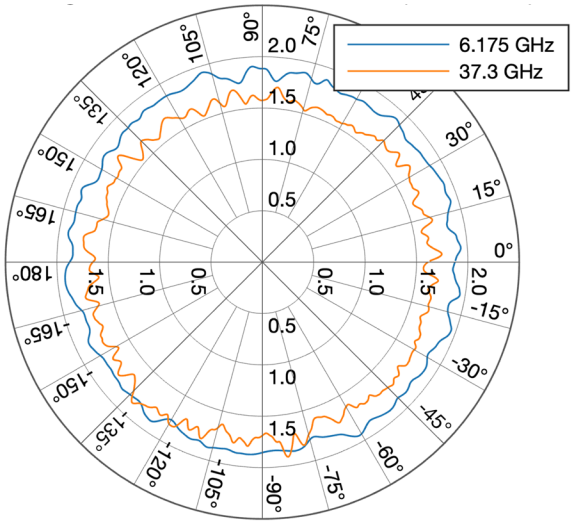

Figure 9 - MIMO capacity gains over CPE antenna orientations with 12 dB SNR at indoor test position 12 with 4λ (TX) and 4λ (RX) antenna separation [12]

An example of the angle of arrival (AoA) estimation is shown in Figure 10 in the form of power angular profiles (PAPs) for indoor TP12 (for both frequencies) Figure 10. Although the MIMO capacity gain could not be optimized in this case, optimizing the CPE orientation could still improve the CPE antenna gain, as for instance in TP12, most of the powers arrives between 110° and 130° azimuth. Here, a MIMO antenna with moderate gain in this direction would be beneficial by increasing the mean received power. Since the current measurements use omni-directional antennas, the estimated MIMO gain values are valid for omni-directional antennas only. Therefore, the impact of directive antennas on the MIMO gain would subject to further investigations.

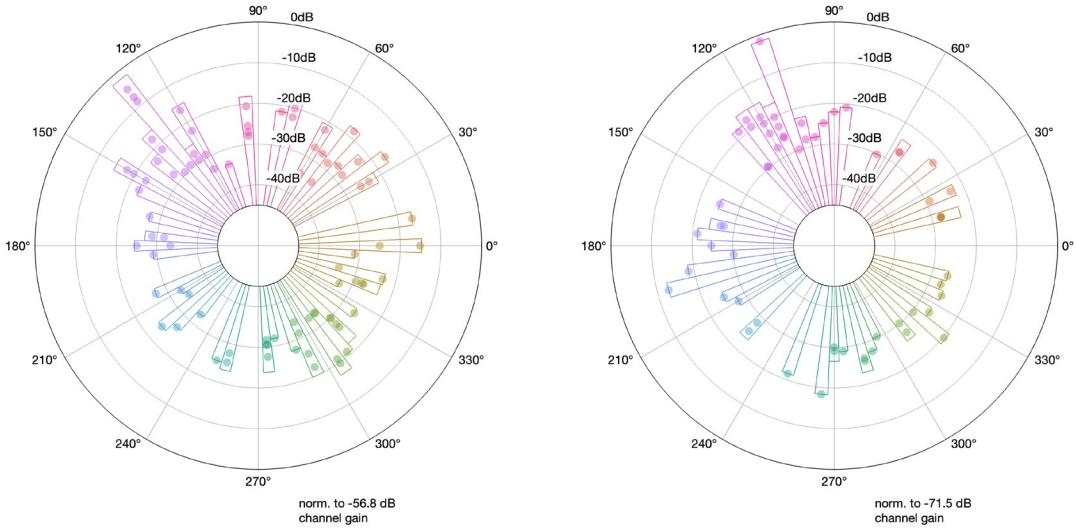

Figure 10 - Power angular profiles at indoor TP 12 at (a) 6 GHz; and (b) 37 GHz [12]

5.4. Correlations between MIMO Capacity Gain and Other Channel Characteristics

A deeper analysis is provided in this subsection about how the MIMO capacity gain is related to or explained by other channel characteristics. The cross-correlation coefficient between the mean MIMO capacity gain, variation of MIMO capacity gain, channel covariance, small-scale fading Rician *K*-factor, RMS-DS, RMS-AS, and number of MPCs in an indoor environment at 6 and 37 GHz are provided in Table 3 and Table 4, respectively. The correlation coefficients in an O2I environment are listed in Table 5 and Table 6. For any given two vectors $A_1$and A_2, the cross-correlation coefficient ρ_{A_1,A_2} follows:

$$\rho_{A_1,A_2} = \frac{E[(A_1-\mu_{A_1})(A_2-\mu_{A_2})]}{\sigma_{A_1}\sigma_{A_2}}, \quad (5)$$

where μ's and σ's are the average and standard deviation of the vectors. ρ ranges from -1 to 1, close to -1 means two vectors are negatively correlated, equal or close to zero indicates the two vectors are uncorrelated, and close to 1 means two vectors are positively correlated.

Table 3 - Correlations between channel characteristics at 6 GHz in an indoor scenario [12]

6 GHz	MIMO capacity gain	Variation (80-20)	Covariance	*K*-factor	RMS-DS	RMS-AS	# of MPCs
MIMO capacity gain	1.00	-0.61	-0.83	-0.50	0.67	0.38	0.71
MIMO capacity gain variation (80-20)	-0.61	1.00	0.82	0.41	-0.77	-0.24	-0.81
Covariance (dB)	-0.83	0.82	1.00	0.61	-0.90	-0.52	-0.95
***K*-factor (dB)**	-0.50	0.41	0.61	1.00	-0.55	-0.65	-0.59
RMS-DS (ns)	0.67	-0.77	-0.90	-0.55	1.00	0.34	0.95
RMS-AS (°)	0.38	-0.24	-0.52	-0.65	0.34	1.00	0.44
# of MPCs	0.71	-0.81	-0.95	-0.59	0.95	0.44	1.00

Table 4 - Correlations between channel characteristics at 37 GHz in an indoor scenario [12]

37 GHz	MIMO capacity gain	Variation (80-20)	Covariance	*K*-factor	RMS-DS	RMS-AS	# of MPCs
MIMO capacity gain	1.00	-0.30	-0.91	-0.84	0.19	0.55	0.56
MIMO capacity gain variation (80-20)	-0.30	1.00	0.52	0.39	-0.30	-0.23	-0.61
Covariance (dB)	-0.91	0.52	1.00	0.86	-0.31	-0.52	-0.74
***K*-factor (dB)**	-0.84	0.39	0.86	1.00	-0.34	-0.47	-0.67
RMS-DS (ns)	0.19	-0.30	-0.31	-0.34	1.00	0.06	0.77
RMS-AS (°)	0.55	-0.23	-0.52	-0.47	0.06	1.00	0.27
# of MPCs	0.56	-0.61	-0.74	-0.67	0.77	0.27	1.00

Table 5 - Correlations between channel characteristics at 6 GHz in an O2I scenario

6 GHz	MIMO capacity gain	Variation (80-20)	Covariance	*K*-factor	RMS-DS	RMS-AS	# of MPCs
MIMO capacity gain	1.00	-0.63	-0.63	-0.52	0.26	0.23	0.41
MIMO capacity gain variation (80-20)	-0.63	1.00	0.68	0.50	-0.53	-0.39	-0.60
Covariance (dB)	-0.63	0.68	1.00	0.54	-0.50	-0.34	-0.59
***K*-factor (dB)**	-0.52	0.50	0.54	1.00	-0.44	-0.39	-0.55
RMS-DS (ns)	0.26	-0.53	-0.50	-0.44	1.00	0.52	0.86
RMS-AS (°)	0.23	-0.39	-0.34	-0.39	0.52	1.00	0.57
# of MPCs	0.41	-0.60	-0.59	-0.55	0.86	0.57	1.00

Table 6 - Correlations between channel characteristics at 37 GHz in an O2I scenario

37 GHz	MIMO capacity gain	Variation (80-20)	Covariance	*K*-factor	RMS-DS	RMS-AS	# of MPCs
MIMO capacity gain	1.00	0.02	-0.70	-0.87	0.20	0.59	0.58
MIMO capacity gain variation (80-20)	0.02	1.00	0.55	0.15	-0.33	-0.10	-0.43
Covariance (dB)	-0.70	0.55	1.00	0.79	-0.47	-0.44	-0.77
***K*-factor (dB)**	-0.87	0.15	0.79	1.00	-0.31	-0.59	-0.72
RMS-DS (ns)	0.20	-0.33	-0.47	-0.31	1.00	0.03	0.28
RMS-AS (°)	0.59	-0.10	-0.44	-0.59	0.03	1.00	0.45
# of MPCs	0.58	-0.43	-0.77	-0.72	0.28	0.45	1.00

The mean MIMO capacity gain is negatively correlated with its variation (between 20th and 80th percentiles) with a correlation coefficient of -0.61 at 6 GHz and -0.3 at 37 GHz indoors. This is because the average MIMO capacity gain is small when the MPCs are sparse in an environment, where the channel diversity is insufficient and MIMO capacity gain may vary over CPE orientation, frequency, or test positions.

The channel covariance matrix R is another measure of propagation channel diversity, which follows:

$$R = 10 \times log_{10}\{E[hh^H]\}, \quad (6)$$

where h column-wise stacking the channel transfer function matrix H into a vector, $E[\cdot]$ is the expectation, and $\{\cdot\}^H$ denotes a conjugate transpose. An example of R is shown in Figure 11. Values close to 0 dB indicate the channels are strongly correlated, such as the values on the diagonal. Small values indicate channels between TX-RX antenna pairs are uncorrelated. Most of the values off the diagonal are small, revealing the channels are loosely correlated and the diversity of the channels is high, which yields a high MIMO capacity gain. This is supported in Table 3 and Table 4 with a -0.91 at 37 GHz or -0.83 at 6 GHz correlation coefficient between channel covariance and MIMO capacity gain.

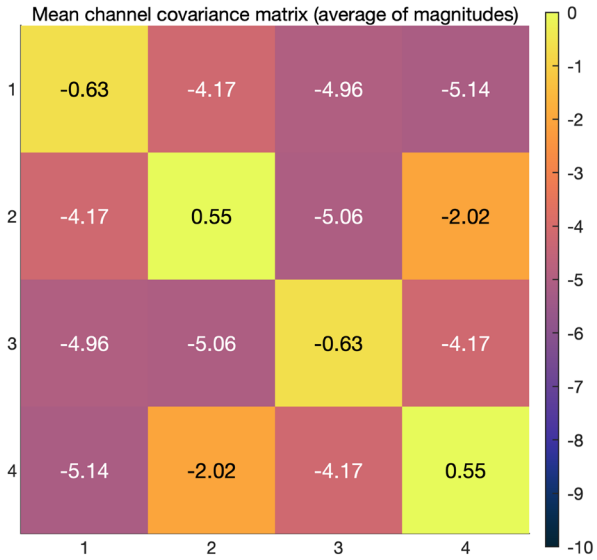

Figure 11 - Example channel covariance matrix in dB at 6 GHz with 4λ antenna spacing indoors at TP 12 [12]

The Rician K-factor in decibels quantifies the envelop power ratio of the dominant path over the sum of all other MPCs. A high K-factor corresponds to strong LOS channel, which the MIMO capacity gain is relatively small. The correlation results in Table 3 and Table 4 agree with the above analysis with a negative correlation coefficient.

The RMS-AS and RMS-AS evaluate the channel dispersion in the angular and delay domains. The MIMO capacity gain versus RMS-AS is provided in Figure 12. The mean MIMO capacity gain increases with RMS-AS when RMS-AS is smaller than 100°, it no longer increases when RMS-AS is larger than 100°. Higher frequency shows a stronger correlation.

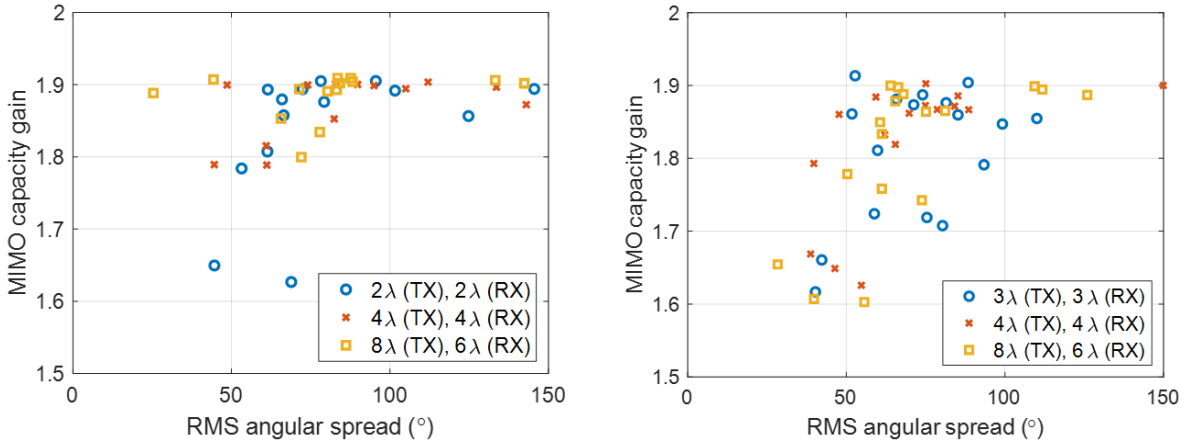

Figure 12 - MIMO capacity gain versus RMS-AS indoors at 6 GHz [12]

The last row in Table 3 and Table 4 is the number of MPCs above a 30 dB MPC threshold. It is the most direct measure of multipath statistics. The more MPCs a channel has (richer scattering environment), the higher the MIMO capacity gains.

6. Conclusion

Deploying MIMO and MU-MIMO, considering MIMO array size and number of MU-MIMO air layers is a tradeoff between cost and performance for MNOs and MSOs in FWA network planning. MIMO not only increases the antenna gain that compensates for high path loss but also increases channel capacity by utilizing the diversity of the propagation channel. In this study, we designed a 2×2 MIMO channel sounder, proposed a method to evaluate MIMO channel capacity gain, and experimentally studied the capacity gain from SISO to MIMO in the specific propagation channels in an indoor-office and residential house outdoor-to-indoor environments. The MIMO capacity gain is theoretically 2 with a 2×2 MIMO, but practically it only achieved 1.7 when the channel diversity is poor such as in the O2I environment in LOS condition. It achieved 1.9 in a rich scattering environment. The MIMO capacity gain is not strongly related to the antenna spacing with our measured range from 2λ to 8λ. The MIMO capacity gain is also compared with CPE orientation. It is unnecessary to optimize CPE orientation in a rich scattering environment. Finally, the MIMO capacity gain is compared with many channel characteristics. It is positively correlated with the number of MPCs, RMS-AS, and RMS-DS. The MIMO capacity gain is negatively correlated with the variation of MIMO capacity gain, channel covariance, and small-scale fading Rician *K*-factor.

Abbreviations

AoA	angle of arrival
AP	access point
BS	base station
CIR	channel impulse response
CPE	customer premises equipment
CTF	channel transfer function
FCC	Federal Communications Commission
FFT	fast Fourier transform
FWA	fixed wireless access
LOS	line of sight
MIMO	multiple-input multiple-output
MNO	mobile network operator
MPC	multipath component
MSO	multiple-system operator
MU-MIMO	multi-user MIMO
NLOS	non-LOS
O2I	outdoor-to-indoor
PAP	power angular profile
PDP	power delay profile
RMS	root mean square
RMS-AS	RMS angular spread
RMS-DS	RMS delay spread
RX	receiver
SIMO	single-input multiple-output
SISO	single-input single-output
SNR	signal-to-noise ratio
TP	test position
TX	transmitter
VCA	virtual circular array

References

[1] Code of Federal Regulations, Title 47, Part 15.401, FCC. Online Available: https://www.ecfr.gov/current/title-47/chapter-I/subchapter-A/part-15/subpart-E/section-15.401.

[2] Code of Federal Regulations, Title 47, Part 30.5, FCC. Online Available: https://www.ecfr.gov/current/title-47/chapter-I/subchapter-B/part-30#p-30.5.

[3] D. Viorel, R. Sun, S. Patel, G. Hart, "Technical Analysis on Rural 5G Fixed Wireless Access for Rural Networks in Sub-7 GHz Bands," White Paper, CableLabs, Nov. 2022. Online Available: [Link]

[4] D. Viorel, R. Sun, S. Patel, G. Hart, "Comparative Technical Analysis for 5G Fixed Wireless Access Rural Networks (2.6, 3.7 and 6.4 GHz)," SCTE Cable-Tec Expo 2022, Philadelphia, PA, 19-22 Sept. 2022. Online Available: [Link]

[5] S. Patel, D. Viorel, R. Sun, "Rural 5G Fixed Wireless Access. Economics Analysis and Methodology," *SCTE Cable-Tec Expo 2022*, Philadelphia, PA, 19-22 Sept. 2022. Online Available: [Link]

[6] D. Viorel, R. Sun, S. Patel, "5G FWA Technical Performance Analysis for Mid-Band Small Cell Networks,"

White Paper, CableLabs, Sept. 2021. Online Available: [Link]

[7] S. Patel, D. Viorel, R. Sun, "Economics of Small Cell-Based Fixed Wireless Access," Strategy Brief, CableLabs, Sept. 2021. Online Available: [Link]

[8] R. Sun, D. Viorel, W. Keusgen, "Indoor Channel Multipath Components Statistics and Spatial Correlation in 6 and 37 GHz Bands," *2022 IEEE Global Communications Conference Workshops (GC Wkshps)*, pp. 1298-1303, Rio de Janeiro, Brazil, 4-8 Dec. 2022.

[9] R. Sun, D. Viorel, W. Keusgen, "Outdoor-to-Indoor Loss Measurement for Rural/Suburban Residential Scenario at 6 and 37 GHz," *17th European Conference on Antennas and Propagation (EuCAP 2023)*, pp. 1-5, Florence, Italy, 26-31 March 2023.

[10] R. Gebremedhin, R. Sun, D. Viorel, W. Keusgen, "Frequency Domain Channel Characteristics in an Outdoor-To-Indoor Environment at 6 and 37 GHz," *2024 18th European Conference on Antenna and Propagation (EuCAP)*, Glasgow, United Kingdom, pp.1-5, 17-22 March 2024.

[11] R. Sun, D. Viorel, W. Keusgen, R. Gebremedhin, "Empirical Path Loss Model and Small-Scale Fading Statistics in an Indoor Office Environment in 6 and 37 GHz Shared Bands," *2024 18th European Conference on Antenna and Propagation (EuCAP)*, Glasgow, United Kingdom, pp. 1-5, 17-22 March. 2024.

[12] R. Sun, W. Keusgen, D. Viorel, "MIMO Channel Capacity Measurements in an Indoor-office Environment at 6 and 37 GHz," *2024 IEEE Global Communications Conference Workshops (GC Wkshps)*, submitted, Cape Town, South Africa, Dec. 2024.

[13] R. Gebremedhin, W. Keusgen, D. Viorel, R. Sun, "MIMO Channel Capacity Measurements in an Outdoor-to-Indoor Environment at 6 and 37 GHz," *2024 IEEE 99th Vehicular Technology Conference (VTC-2024 Spring)*, pp 1-7, Singapore, June 2024.

[14] D. Viorel, R. Sun, W. Keusgen, "FWA Propagation in 6 and 37 GHz Bands," *SCTE Tec-Expo 2024*, Atlanta, GA, 24-26 Sept. 2024.